Optimized Capture-Solenoid Field for a Muon Accelerator Front End

K. T. McDonald,[1] H. K. Sayed,[2] J. S. Berg,[2] H. G. Kirk,[2] and R. B. Palmer[2]

[1] *Joseph Henry Laboratories, Princeton University, Princeton, NJ 08544, USA*
[2] *Brookhaven National Laboratory, Upton, NY 11973, USA*

(Dated: (March 26, 2014))

In a muon accelerator complex, a target is bombarded by a multi-MW proton beam to produce pions that decay into muons, which are thereafter bunched, cooled, and accelerated. The Front End of the complex captures and manipulates the phase space of those pions, and that of the muons into which they decay, in a solenoidal magnetic channel to maximize the number of muons within the acceptance of the downstream acceleration system. For a channel of a given radius, more particles are captured by a higher solenoid field, with higher-transverse-momentum particles captured if the magnetic field at the target is higher than that in the subsequent channel. This improvement in the capture efficiency is associated with an increase in the longitudinal phase space of the captured particles, which can be disadvantagous for transport through RF cavities in the complex. Simulations are presented which show that a relatively rapid decrease (taper) from high to low field along the Front End channel optimizes its performance.

PACS numbers: 41.75.-i, 41.75.Ak, 41.75.Cn, 41.85.-p, 41.85.Ja, 41.85.Ct

I. INTRODUCTION

The realization that the concept of ionization cooling [1] is best applied to muons [2] led to proposals for muon accelerators, the Muon Collider and the Neutrino Factory, that use intense muon beams to study the physics of elementary particles at both the intensity and energy frontiers. At a Muon Collider, bunches of μ^+ and μ^- collide at energies as high as several TeV [3–12]. At a Neutrino Factory, intense neutrino beams derive the decay of muons which have been accelerated to energies of order 10 GeV [12–20].

Muons for a muon-accelerator complex are from the decay of pions produced by bombarding a target with a high-power proton beam. These muons are to be delivered into a specified (normalized) acceptance (also called admittance [21]) for the muon accelerator, taken here to be 150 mm = 0.053 eV-s (per bunch for a train of ≈ 20 bunches of each sign) for the longitudinal acceptance and 30 mm for the transverse acceptance.

A. Emittance Conventions

Interactions between the particles are ignored in this study, such that it suffices to describe them as populating a six-dimensional phase space. The phase-space variables used here are x, p_x, y, p_y, E and t, with z as the independent variable in a Hamiltonian description, following Appendix B of [22]. Here, $\mathbf{p}$ is the canonical momentum $\mathbf{P} - q\mathbf{A}/c$ where $\mathbf{P} = \gamma m\mathbf{v}$ is the kinetic momentum of a particle of (rest) mass m, velocity $\mathbf{v}$ and electric charge q, $\mathbf{A}$ is the (azimuthally symmetric) vector potential (in the Coulomb gauge), $\gamma = 1/\sqrt{1 - v^2/c^2}$, E is the total energy, and c is the speed of light in vacuum. The extent of the muons in phase space is characterized by normalized, rms (root mean square) emittance [23–28], and the acceptance of a device is the largest particle emittance that it can accommodate. The longitudinal normalized emittance is $\epsilon_\parallel = [\Sigma_{tt}\Sigma_{EE} - \Sigma_{tE}^2]^{1/2}/(mc)$, and the transverse normalized emittance is $\epsilon_\perp = [\det(\Sigma_T)]^{1/4}/(mc)$, where Σ_T is the 4×4 sub-block of the covariance matrix Σ in the kinetic variables x, P_x, y, and P_y. The covariance matrix Σ of the phase space variables ξ_i has matrix elements

$$\Sigma_{\xi_i,\xi_j} = \langle \xi_i \xi_j \rangle - \langle \xi_i \rangle \langle \xi_j \rangle. \tag{1}$$

B. Transverse Distributions in a Solenoid Channel

Both positively and negatively charged secondary particles from the target are captured in a solenoid-magnet channel of radius R and axial field B, and move on helical trajectories with radius $r = cP_\perp/qB$, where c is the speed of light, $P_\perp$ is the particle transverse momentum, and q is the magnitude of the charge of the particle. For a target with transverse extent small compared to the channel radius R, particles (of charge q equal in magnitude to that of an electron) produced with transverse momentum up to $P_{\perp,\max} \approx qBR/2c$ such that particles with $r < R/2$, would be captured independent of their longitudinal momentum. If $P_{\perp,\max} \gg \langle P_\perp \rangle$ ($(B \gg 2c\langle P_\perp \rangle /qR)$) then $\sigma_{P_\perp} \approx \langle P_\perp \rangle$, and a typical helical trajectory extends to maximum distance $d \approx 2c\langle P_\perp \rangle /qB$ from the axis if the solenoid channel.

Although the secondary particles are created in a volume with small radial extent, and hence nominally small transverse emittance, their spread in energy and axial point of origin is substantial. As they propagate on helical trajectories in the solenoid channel their transverse spatial distribution effectively fills the entire area of radius d such that $\sigma_r \approx d$, and the transverse emittance rises with distance along the solenoid channel to

an asymptotic value, given in cm for captured muons by

$$\epsilon_\perp \approx \frac{\sigma_r \sigma_{P_\perp}}{m_\mu c} \approx \frac{2\langle P_\perp \rangle^2}{eBm_\mu}, \qquad (2)$$

where $-e$ is the charge of an electron. The argument leading to eq. (2) assumed that $B \gg 2c\langle P_\perp \rangle / eR$, for which $P_{\perp,\max} \gg \langle P_\perp \rangle$.

The asymptotic rms emittance in a solenoid channel can also be understood by considering the evolution of the distribution in transverse phase phase in a rotating (Larmor) frame where the Poincaré maps for particles with different energy and different transverse amplitude rotate (and distort) over the transverse phase space at different rates, resulting in a "swept-out" rms emittance given by eq. (2) with $\langle P_\perp \rangle$ replaced by $\sigma_{P_\perp}$. Related effects in injection systems with quadrupole transport are discussed in [29].

The secondary-pion spectrum peaks at low longitudinal momentum ($\approx$ 100 MeV/c), while the average transverse-momentum is $\approx$ 250 MeV/c independent of the pion energy. If the solenoid channel had 1.5-T field and 30-cm radius at the target, the maximum captured transverse momentum would be only $P_{\perp,\max} =$ 67.5 MeV/c, which is small compared to the average transverse momentum of the secondary particles, resulting in low capture yield. To improve the fraction of secondary particles that are captured, a stronger magnetic field is applied on the target.

C. Adiabatic Field Taper

If the axial magnetic field varies slowly with axial position, the magnetic flux through the helical trajectory of a charged particle (as well as the magnetic moment of its orbital motion) is an adiabatic invariant [30–32]; $Br^2 = c^2 P_\perp^2 / B \approx$ constant. If, say, the solenoid field on the target were $B_i = 20$ T (near the limit of technical feasibility) and the field in the subsequent channel (called the Decay Channel in the following) were $B_f = 1.5$ T, then the average transverse momentum, 250 MeV/c, of pions at the target would be adiabatically transformed to 68.5 MeV/c in the Decay Channel and the latter would accept a substantial fraction of all pions produced at the target. Such considerations led to the specification of a high magnet field on the target [10, 33], followed by a "taper" of the field down to the lower value B_f in the Decay Channel, and simulations of the yield of muons at the end of such a channel [34] indicated that a field of $B_i \approx 20$ T on the target is optimal (according to the criteria of that study). The taper length in these studies was only ≈ 3 m, while taper lengths of 18 m were considered beginning in [17], in part because the growth of transverse emittance due to the decay of pions to muons is less if the decays occur in higher magnetic fields.

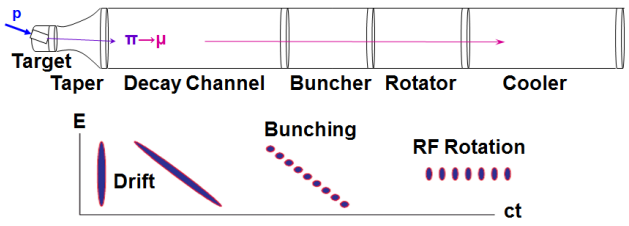

FIG. 1. Layout of the Front End (prior to net acceleration of muons) of a muon accelerator, indicating schematically the target, magnetic-field taper, Decay Channel, Buncher, Phase Rotator and (ionization) Cooler. The transformation of the initial macrobunch with large energy spread produced at the target into a train of microbunches with common central energies is sketched in the lower part of the figure.

D. Manipulation of Longitudinal Phase Space

While the solenoid channel transports charged particles of any longitudinal momentum $P_\parallel$ if $P_\perp < P_{\perp,\max}$, acceleration of these particles in rf cavities requires them to have a limited spread of $P_\parallel$. The particles within the transverse acceptance of the Decay Channel are formed by the Front End [35] into bunches for later acceleration in four steps, illustrated in Fig. 1: a single bunch of secondary particles with large energy spread is produced at the target by protons with a narrow time spread; as this bunch drifts (and the pions and Kaons decay) in the Decay Channel those particles with smaller $\beta_z = v_z/c$ fall behind to produce an energy-time correlation; a series of rf cavities called the Buncher decomposes the macrobunch into a train of microbunches whose central particles retain the energy-time correlation; a second series of rf cavities are phased such that lower energy microbunches are accelerated while higher energy bunches are decelerated resulting in a final train of bunches with a common central energy. The fourth step is called phase-energy rotation [36, 37] (which bunch manipulation is a variant of that performed at $\overline{p}$ sources [38]), and the set of rf cavities that perform this action is called the Phase Rotator.

While the energy of secondary particles is unaffected by the variation of the magnetic field in the taper region, their longitudinal momenta and axial velocites increase, and the longitudinal emittance increases, which has a subtle effect on the number of muons transmitted through the Buncher and Phase Rotator. This effect is the main topic of this paper.

The transverse emittance decreases while the longitudinal emittance increases during transport through the tapered magnetic field. Such an emittance exchange is not possible in systems that can be described by a "linear" canonical transformation [39], but the beam transport in the Front End is "nonlinear" (nonsymplectic).

Studies such as [34, 40, 41] did not consider the longitudinal acceptance of the Front End when optimizing the Target System. First evidence was given in [42] that

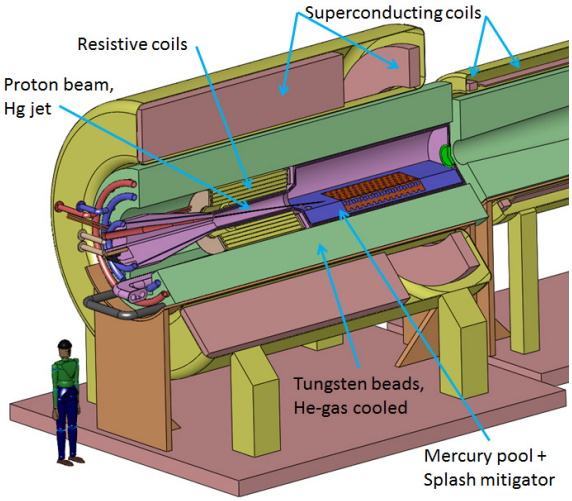

FIG. 2. Neutrino Factory/Muon Collider Target System.

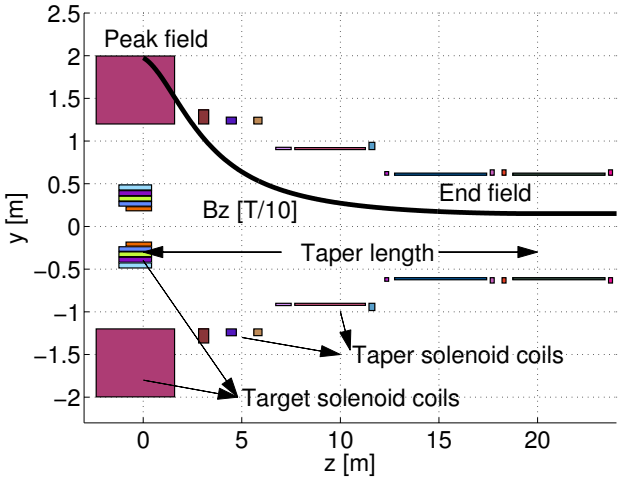

FIG. 3. Target System solenoid coils, and axial magnetic field (divided by 10) for the nominal configuration.

a relatively rapid, nonadiabatic taper is preferred when the longitudinal acceptance is considered. The systematic studies presented here confirm that a rapid taper to a larger final axial field than 1.5 T in the Decay Channel, Buncher and Phase Rotator improves the yield of "useful" muons for the subsequent muon accelerator.

II. THE FRONT END

The Front End of a muon accelerator considered here is a slight variant of that described in [13, 20, 35].

A. Target System

A 4-MW proton beam (about 3×10^{15} 8-GeV kinetic-energy protons/s) intersects the free mercury jet of velocity 20 m/s, which presents a fresh target to the beam every pulse at 15-Hz repetition rate. The proton beam and mercury jet are tilted with respect to the magnetic axis, as shown in Fig. 2, to minimize reabsorption of low-energy pions as they spiral in the magnetic field B_i on the target. The nominal axial field peaks at $B_i = 20$ T at the target and then tapers down to $B_f = 1.5$ T over 15 m, as illustrated in Fig. 3. The 20-T field on the target is produced by a 15-T superconducting-coil outsert and a 5-T resistive-coil insert [43].

In the present study the initial and final magnetic fields, B_i and B_f, and the axial length L_t of the taper were varied using an analytic model for the axial field, from which the off-axis field (consistent with Maxwell's equations) was deduced as described in Appendix A. Figure 4 shows some of these field profiles.

B. Decay Channel

The Decay Channel follows the taper region of the Target System, and is taken here to be a straight solenoid channel of radius $R = 30$ cm and magnetic field B_f (the chicane described in [35] was not considered). In addition to being the region in which most pions and Kaons decay into muons, the drift of the low-energy particles in the Decay Channel provides the correlation between their energies and times used in the downstream phase rotation [37].

The distance from the target to the end of the Decay Channel was held fixed at 79.6 m in this study. In future studies, where the parameters of the Buncher and Phase Rotator are varied, this distance will be reoptimized.

The field from the the discrete set of solenoids in the

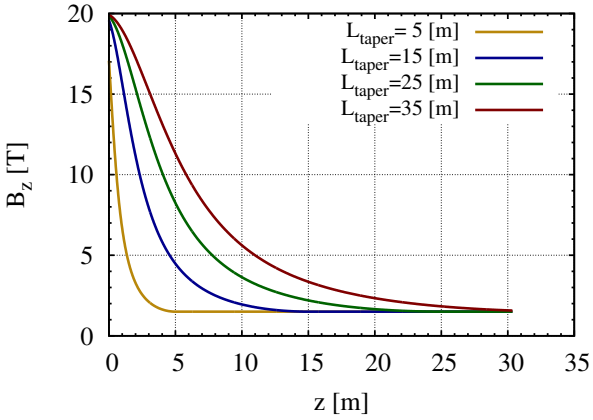

FIG. 4. Axial solenoid field profiles used in the present study with $B_i = 20$ T, $B_f = 1.5$ T, and taper lengths between 5 and 35 m.

Decay Channel introduces stop-bands and nonlinearities that reduce transmission by about 2% compared to a constant solenoid field [44].

C. Buncher

The Buncher [35, 45] considered here has a series of 37 rf cavities with frequencies decreasing from 320 to 232 MHz over a distance of 33 m. The rf gradients increase adiabatically from 3.4 to 8 MV/m as the initial macrobunch of particles is transformed into a sequence of ≈ 40 bunches (≈ 20 of each sign, interleaved with offsets of π in rf phase) which occupy ≈ 60 m along the beamline. The rf frequencies decrease with distance to keep the rf buckets centered on the bunches as the time between bunches increases due to their differing energies.

D. Phase Rotator

The Buncher is followed by a 42-m-long Phase Rotator [35, 45] that transforms the bunches, which have different central energies, into a set with nearly equal energies. It contains 56 rf cavities which have frequencies decreasing from 230 MHz to 202 MHz, all with field gradient of 13 MV/m. The rf-cavity phases are set such that the energies of all the bunches gradually become identical. The rf frequencies decrease so as to maintain these phases as the time between bunches increases due to their energy differences, and that decrease slows as the range of bunch energies is reduced. *This doesn't make sense, as the energy differences decrease with increasing z.*

The result is that muons with an initial momentum range of 80-500 MeV/c are captured into a train of 201-MHz bunches with an average momentum of 232 MeV/c and a momentum spread of 10%.

E. Cooling Channel

In the Neutrino-Factory scenario, the Phase Rotator is followed by a transverse ionization Cooling Channel (the Cooler in Fig. 1). This is a sequence of n =??? identical 75-cm-long cells that focus with alternating solenoids producing a maximum field magnitude on axis of 2.8 T. A 6-m-long section (of what????) is required to match between the constant solenoid field in the Phase Rotator and this alternating field. The cells contains LiH absorbers for ionization cooling and RF cavities that provide longitudinal focusing and restore the energy lost in the absorbers. The RF cavities have a frequency of 201 MHz and an accelerating gradient of 16 MV/m. *The above scenario differs slightly from that in [45]. Do we have a reference for the above?*

III. EFFECT OF THE SOLENOID FIELD PROFILE ON PARTICLE CAPTURE EFFICIENCY

The effect of the solenoid field profile in the taper region just downstream of the target on the performance of the Front End was first studied for the beam just after the target (sec. IIIA), then at the end of the Decay Channel (sec. IIIB), and at the end of the Front End (sec. IIIC). Next, effect of the final solenoid field B_f was studied (sec. IIID). We then examined how the beam distribution and capture at the end of the decay channel is affected by the taper length. Next, we studied how the complete field profile affected the performance of the full system, including the buncher, phase rotation, and ionization cooling. We then describe how the final field affects the capture performance. In these studies the proton bunch length incident on the target was taken to be zero; the effect of that length on the performance of the Front End is considered in sec. IV.

Particle production at the target was simulated using the MARS15(2010) code [46, 47]. Secondary particles were tracked through the subsequent Decay Channel, Buncher, Phase Rotator and Cooling Channel, using the ICOOL code [48].

A. Target Field and Capture

The rms transverse emittance of particles produced in a radially thin target in axial magnetic field B was estimated to grow with propagation in the axial direction to the value given in eq. (2), for a channel of a fixed radius. Much of this emittance growth occurs by the end of the target. The simulation of Fig. 5 shows that the distributions of charged pions, Kaons, and muons in transverse phase space (with radial aperture of 30 cm) at the end if the target is more elongated, with larger rms area, for lower fields. Figure 6 shows the rms transverse emittance for the distribution of Fig. 5 as a function of the magnetic field B at the target, with the emittance varying roughly as $1/B$ as predicted by eq. (2) for $B \gg 2c\langle P_\perp\rangle/eR \approx 6$ T with $\langle P_\perp\rangle = 250$ MeV/c and $R = 30$ cm. The falloff near 10 T indicates that at these fields the rms emittance growth with distance had not reached its asymptotic value by the end of the target.

Figure 6 also shows that for a given radial aperture more particles are captured by higher fields, at which the helical trajectories of higher transverse-momentum particles lie within the acceptance. Essentially all secondary particles would be captured by a 50-T field and a 30-cm-radius aperture.

B. Muon Yield at the End of the Decay Channel

The capture of pions/muons from the target by the Front End is improved if the field B_i on the target is

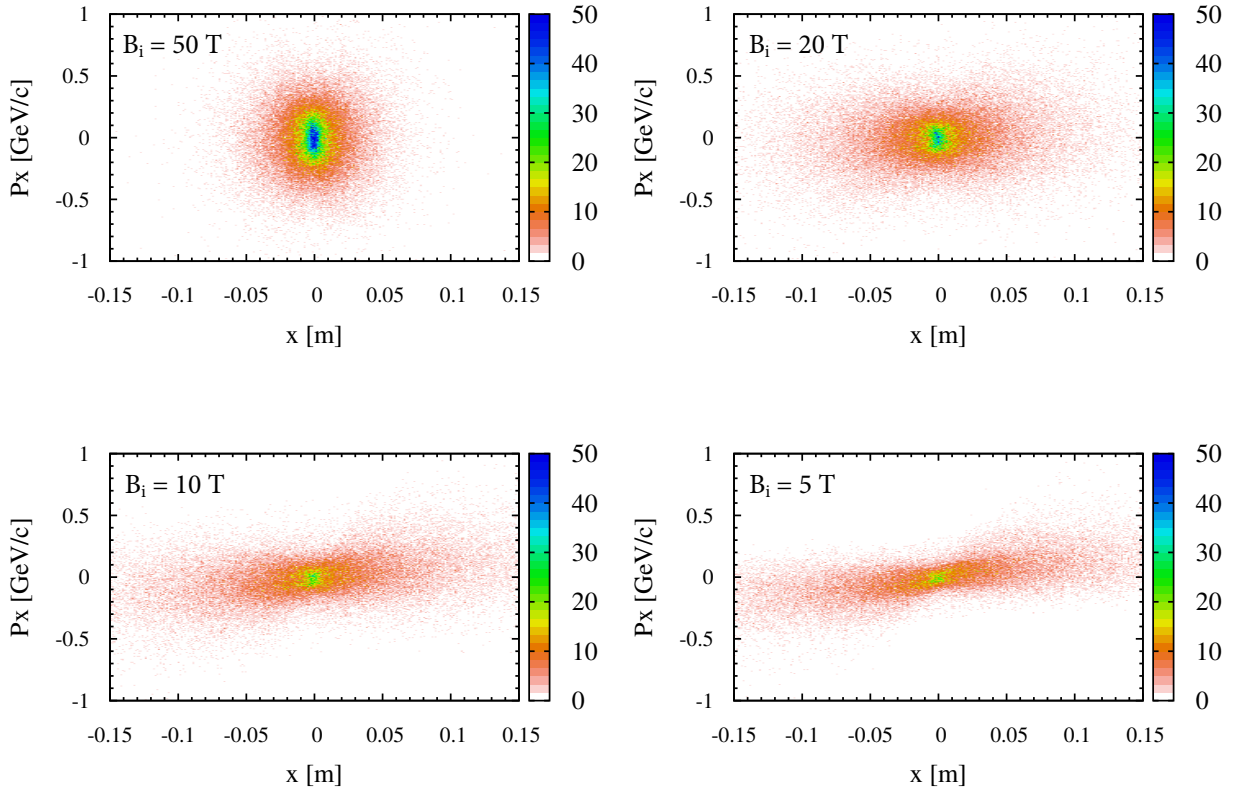

FIG. 5. Distributions of pions, Kaons, and muons at the end of the mercury target in the transverse phase space x-p_x, where p_x is the canonical momentum, for solenoid target fields B_i varying from 5 to 50 T.

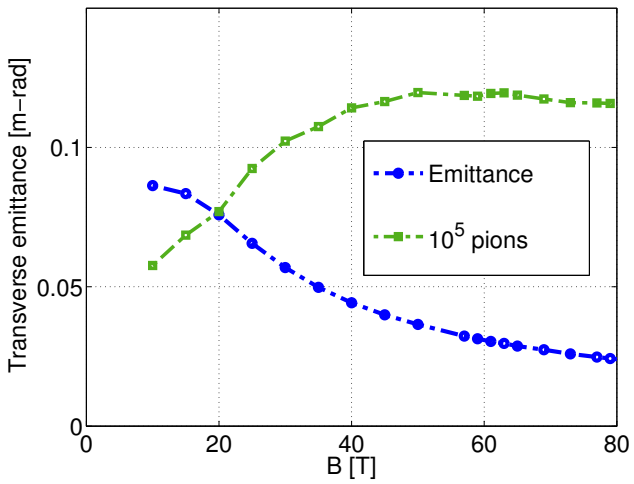

FIG. 6. The rms transverse emittance of secondary particles (blue curve), and the number of particles within a 30-cm radial aperture (green curve), at the end of the target in a MARS simulation.

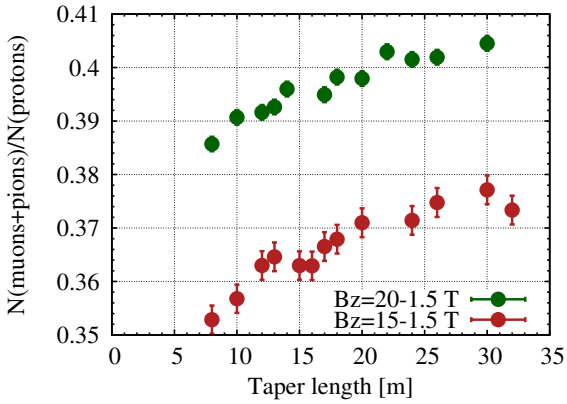

FIG. 7. The number of positively charged muons and pions with kinetic energy from 80 to 140 MeV, per beam proton, counted 80 m downstream from the end of the target, *vs.* taper length for fields $B_i = 15$ and 20 T.

much larger than the field B_f in the bulk of the Front End, as discussed in sec. I. Nominal values of $B_i = 20$ T and $B_f = 1.5$ T existed at the start of this study. It seemed natural to adoprt a slow decrease (taper) with position from field strength B_i to B_f so as to maintain an adiabatic invariance for the particle trajectories. Such adiabaticiy holds when the length scale over which the magnetic field changes is large compared to the period

(betatron wavelength) of the helical trajectory of a particle, *i.e.*,

$$\frac{2\pi c P_z}{qB^2}\frac{dB}{dz} \ll 1. \quad (3)$$

To study the effect of the taper length on the capture efficiency of useful pions/muons, defined to have with a kinetic energy between 80 and 140 MeV, secondary particles from the target (according to a MARS simulation) were tracked (in an ICOOL simulation) 80 m downstream from the target, to a plane near the end of the Decay Channel. Fields $B_i = 15$ and 20 T at the target, and taper lengths varying from 5 to 40 m down to field $B_f = 1.5$ T were considered, with results shown in Fig. 7. A longer, more adiabatic taper increases the number of useful muons at the end of the Decay Channel, while the number of pions and muons at the end of the Decay Channel was decreased by about 8% when the target field from $B_i = 20$ to to 15 T.

However, it may be that advantage of a slow taper in improving the yield of useful muon at the end of the Decay Channel results in an increase in the longitudinal emittance, such that the transmission through the Buncher and Phase Rotator is reduced. In this case a shorter taper may be preferred.

C. Taper Length and Longitudinal Phase Space

Particle production and transport to the end of the Decay Channel were simulated for taper lengths of 4 and 40 m with $B_i = 20$ T and $B_f = 1.5$ T, resulting in the longitudinal-phase-space distributions at $z = 20$, 40 and 80 m shown in Figs. 8 and 9. A notable feature is that the bunch length at a given energy E is shorter, and the density of particles in longitudinal phase space is higher, for the shorter taper, which can lead to better beam transport through the subsequent Buncher and Phase Rotator.

The time spread of the muon beam at the end of the Decay Channel as a function of taper length was computed as the weighted average of the rms with in time for 250 bins in total energy E from $m_\mu c^2$ to 1 GeV (with weighting by the number of muons in each bin). Results for taper lengths from 8 to 40 m are shown in Fig. 10. The bunch length increases by a factor of two over this range, approximately linearly with the taper length. The corresponding increase in rms longitudinal emittance with increasing taper length is shown in Fig. 11. These longitudinal emittances are all large compared to the acceptance of 0.053 eV-s of the muon accelerator downstream, so the beam at the end the Decay Channel is decomposed into bunches of appropriate emittance in the Buncher.

The original purpose of the taper was to reduce the transverse momentum (and hence the transverse velocity) of the particles in an adiabatic transition from high to low axial magnetic fields. The time spread of particles of a given energy depends on the spread of their axial velocities, which is larger when their transverse velocites are larger in the higher magnetic field at the beginning of the taper. Hence, longer tapers (in which particles spend more time in higher fields) lead to a larger time spread in the beam at the end of the Decay Channel.

The transit time of a particle with transverse momentum $P_\perp \ll P$ can be approximated as

$$t = \int_0^z \frac{dz'}{v_z} \approx \frac{E}{c^2 P}\int_0^z dz' \left(1 + \frac{P_\perp^2}{2P^2}\right), \quad (4)$$

such than for an adiabatic field taper where $P_\perp^2(z)/B_z(z) = P_{\perp i}^2/B_i$, the difference Δt between the arrival time at a position z of a particle with a nonzero transverse momentum and one with zero transverse momentum but the same total momentum P and total energy E is

$$\Delta t \approx \frac{P_{\perp i}^2 E}{2c^2 P^3}\int_0^z \frac{B_z(z')}{B_i}\, dz', \quad (5)$$

For a given initial field $B_i = B_z(0)$ and final field B_f, Δt is a linear function of the taper length. The rms time spread for a bunch of particles (launched at the same time at $z = 0$) follows from eq. (5) on computing the standard deviation of the factor in front of the integral over the beam distribution at $z = 0$.

As the taper becomes shorter and therefore less adiabatic, we expect some growth in transverse emittance to accompany the reduction in longitudinal emittance, as indicated in Fig. 11. This explains the reduced transmission at shorter taper lengths seen in Fig. 7. The relative increase in the square of the rms transverse emittance with a shorter taper is less than the decrease in longitudinal emittance, such that the six-dimensionsal rms emttance is lower for shorter taper lengths.

D. Performance with Buncher, Phase Rotator and Cooling Channel

Only a subset of the muons at the end of the Decay Channel will be captured by the Buncher and Phase Rotation, be subsequently cooled, and finally be within the acceptance of the acceleration system. The ultimate performance of the Front End is therefore defined as the ratio of the number of muons delivered within the acceptance of the muon accelerator to the number of protons on target. To compute the number of accepted muons it is convenient to transform to normalized (Floquet) coordinates (*i.e.,* action-angle variables) [49–51]. In particular, the transverse and longitudinal amplitudes A_T and A_L (defined in secs. 3.3 and 3.3 of [28]; see also [52]) must obey $A_T < 30$ mm and $A_L < 150$ mm for the muons to be accepted.

Optimization of the phases and frequencies of the RF cavities in the Buncher and Phase Rotator, and of the matching section to the Cooling Channel, was essential to optimize the performance of the Front End increasing the

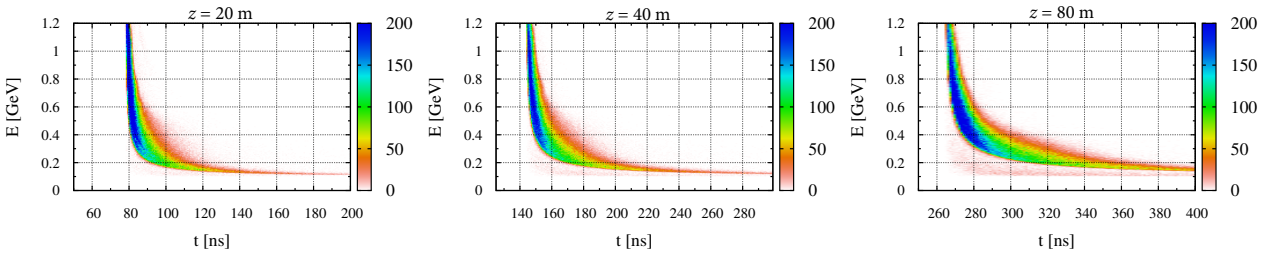

FIG. 8. Longitudinal phase space of pions/muons at $z = 20$, 40 and 80 m for a 4-m-long tapered solenoid.

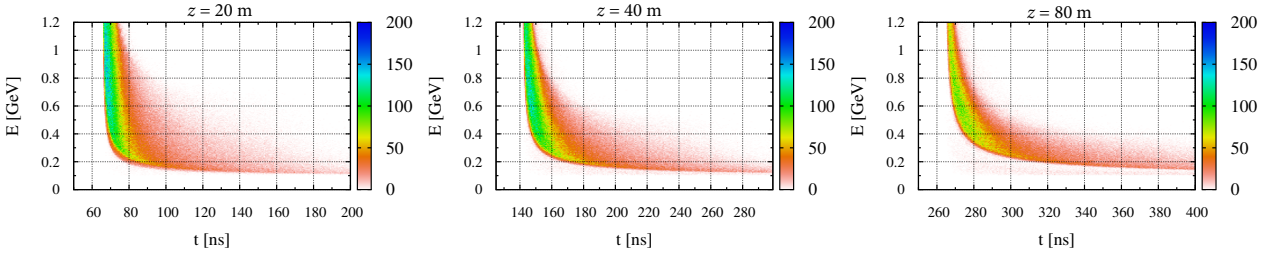

FIG. 9. Longitudinal phase space of pions/muons at $z = 20$, 40 and 80 m for a 40-m-long tapered solenoid.

end field [53], particularly for cases with higher final field B_f. Because the length of the Cooling Channel considered here was not optimized prior to the present study, it was necessary to determine that location along the Cooling Channel that maximized the number of muons within the above acceptance cuts.

Figure 12 shows, for 4- and 40-m taper lengths, longitudinal-phase-space distributions for both the full muon beam at the end of the Decay Channel and the subset of those particles that meet the acceptance criteria. The region of longitudinal phase space where particles are accepted occupies a greater fraction of the total when the taper is shorter.

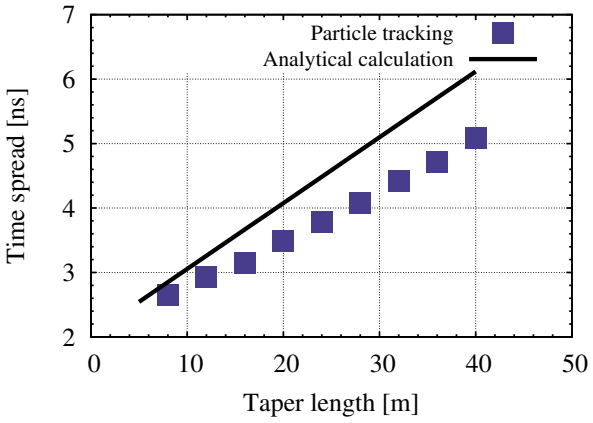

FIG. 10. The rms time spread of the muon beam at the end of Decay Channel as a function of the solenoid taper length. ICOOL simulations are shown with squares, and model results based on eq. (5) are shown by the curve.

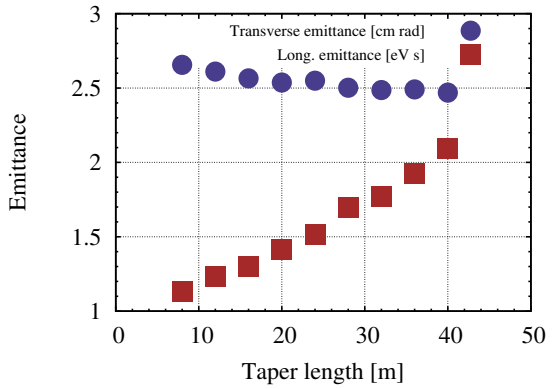

FIG. 11. Transverse and longitudinal emittances of the muon beam at the end of Decay Channel as a function of the solenoid taper length, for the same simulation as in Fig. 10.

Fig. 13 shows the performance of the Front End as a function of taper length for target fields $B_i = 15$ and 20 T, and for final fields $B_f = 1.5$, 2.0, and 2.5 T. For all cases, the performance falls rapidly for taper lengths shorter than 4 m, as then the taper is no longer sufficiently adiabatic. The best performance is obtained with taper length of 5-6 m, beyond which the increase in longitudinal phase volume is larger than the reduction in transverse phase volume and the number of accepted

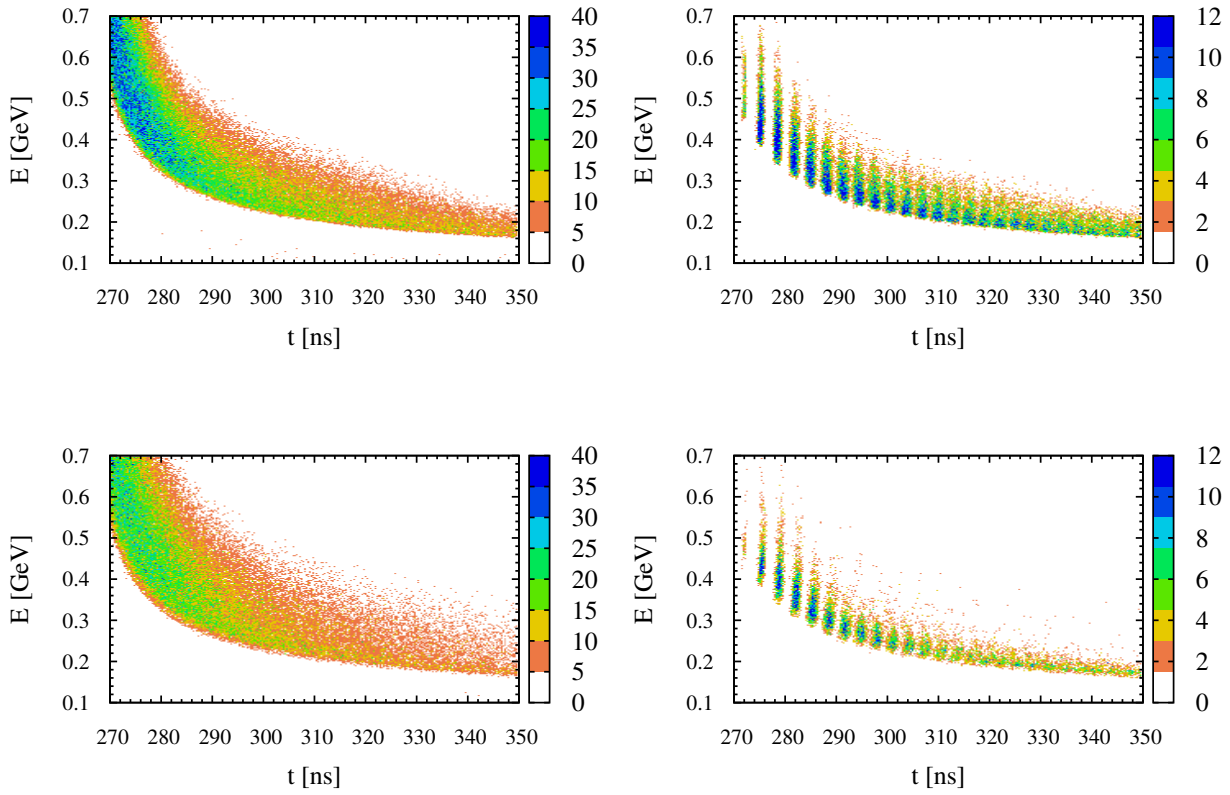

FIG. 12. Longitudinal phase space of the muon beams at the end of the Decay Channel. Top: 4 m taper length; Bottom: 40 m taper length. Left: All muons at the end of the Decay Channel; Right: Muons at the end of the Decay Channel that are captured by the Buncher, Phase Rotator and Cooling Channel.

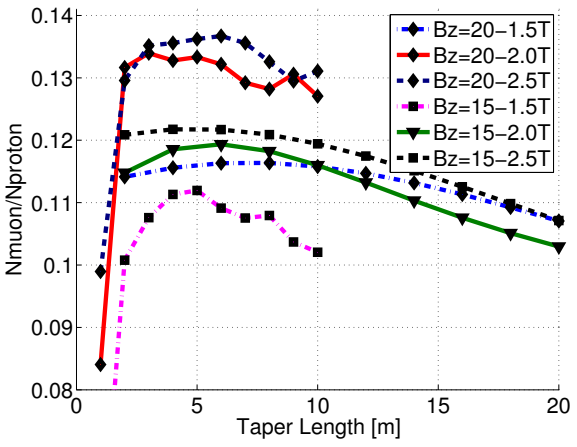

FIG. 13. Ratio of positive muons accepted from the Front End per 8 GeV proton on target, as a function of taper length for target fields $B_i = 15$ and 20 T, and final fields $B_f = 1.5$, 2.0, and 2.5 T.

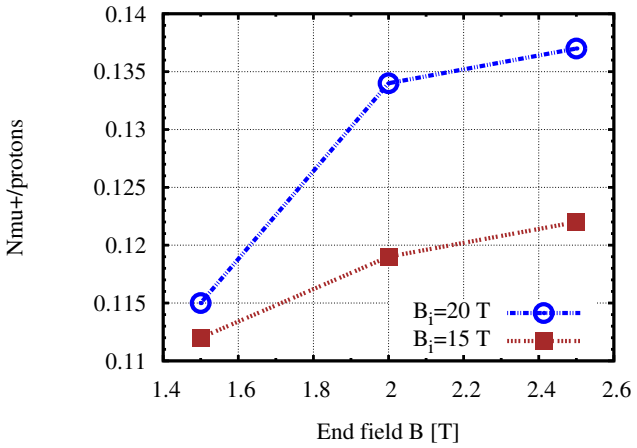

FIG. 14. Accepted positive muons per 8 GeV proton on target as a function of the final field B_f. The target field is $B_i = 15$ or 20 T, and the taper length is 5 m.

muons drops.

Higher fields B_i at the target improve the performance, as shown in Fig. 13, since particles of higher transverse momenta are then captured (for a fixed radial aperture in the Decay Channel).

The strength B_f of the final field determines the maxi-

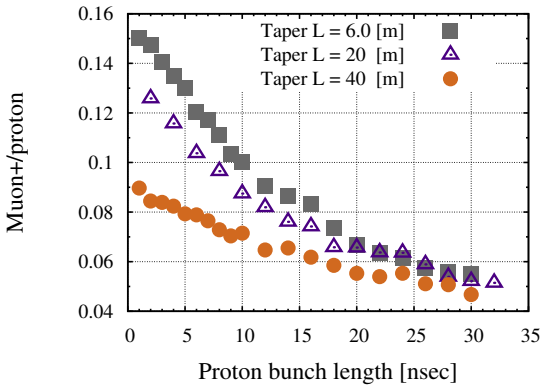

FIG. 15. Accepted muons per incident proton as a function of the proton bunch length for three different taper lengths. The target field is $B_i = 20$ T, and the final field is $B_f = 3.5$ T.

mum captured transverse momentum, and hence the the number of captured particles increases with B_f. Figure 14 shows that the performance with $B_i = 20$ T and 5-m taper length improves with increasing final field B_f by about 20% for every 1-T increase in B_f (and would continue to increase if higher final fields were used)

IV. EFFECT OF PROTON BUNCH LENGTH

The preceeding studies were performed assuming zero time spread for the incident proton bunch. Nonzero time spread of the proton bunch is expected to reduce the capture efficiency of the Front End [54], as this reduces the effectiveness of the Phase Rotator. Hence, the advantage of a short taped found in the previous section will be less for proton bunches bunches of finite time spread.

Figure 15 shows the performance of the Front End as a function of the proton bunch length for three different taper lengths. Performance is reduced by approximately 3% for each 1 ns increase in proton bunch length. For very long incident proton bunch length the performance is about a factor of 3 lower than that for very short bunch length. Muon Collider and Neutrino Factory designs [12] specify 2–3 ns proton bunch lengths, for which a short taper length is advantageous.

V. SUMMARY

Ideally, a system to system to capture secondary particles from a target in a solenoid magnet channel capture particle of all transverse momenta if a sufficiently high field is used. The capture of a system with a lower than optimal magnetic field strength can be improve by use of an an initial high-field solenoidal followed by an adiabatic taper to the lower (final) field. While this configuration increases the range in transverse momentum of the captured particles compared to that of a channel without the initial higher field, it also increases their longitudinal phase area. If the subsequent beam transport includes RF cavities, it is advantageous for the adiabatic reduction in solenoid field to occur rapidly, to minimize the extent of the longitudinal phase space of the captured particles.

Appendix A: TAPER FIELD PROFILE

An axisymmetric magnetic field $\mathbf{B}(r,z)$ can be expressed in terms of its axial field $B_z(0,z)$ according to

$$B_z(r,z) = \sum_n (-1)^n \frac{B_z^{(2n)}(0,z)}{(n!)^2} \left(\frac{r}{2}\right)^{2n} \tag{A1}$$

$$B_r(r,z) = \sum_n (-1)^{n+1} \frac{B_z^{(2n+1)}(0,z)}{(n+1)!n!} \left(\frac{r}{2}\right)^{2n+1}, \tag{A2}$$

where $B_z^{(k)}(0,z)$, is the kth derivative of $B_z(0,z)$ with respect to z.

In this study, the axial field in the taper region, $z_i < z < z_f = z_i + L_t$ was approximated by the analytic form [55]:

$$B_z(0,z) = \frac{B_i}{1 + a_1(z-z_i) + a_2(z-z_i)^2 + a_3(z-z_i)^3} \tag{A3}$$

$$a_1 = -\frac{B_i'}{B_i} \tag{A4}$$

$$a_2 = 3\frac{B_i - B_f}{B_f L_t^2} - \frac{2a_1}{L_t} \tag{A5}$$

$$a_3 = -2\frac{B_i - B_f}{B_f L_t^3} - \frac{a_1}{L_t^2}, \tag{A6}$$

where $B_{i,f}$ are the axial fields at $z_{i,f}$. This form has zero derivative at z_f, $B_f' = dB_z(0,z_f)/dz = 0$. In the present study the parameter a_1 was set to zero, *i.e.*, the axial derivative as also zero at z_i.

While the magnetic fields modeled in the above manner obey Maxwell's equations, it turned out that the shortest tapers considered could not readily be produced by coils of the large radii needed to accommodate internal shielding against radiation damage from secondary particles. Later studies with magnetic fields provided by more practical coil configurations confirm the essential results of the present study as to the advantage of short tapers.

ACKNOWLEDGMENTS

We would like to thank X. Ding, I. Efthymiopoulos, R.C. Fernow, J.C. Gallardo, V.B. Graves, O.M. Hansen, D.V. Neuffer, G. Prior, R. Ryne, N. Souchlas, D. Stratakis amd R.J. Weggel for useful discussions. This effort was supported in part by the Office of High Energy

Physics of the U.S. Department of Energy under Contract No. DE-AC02-98CH10886.

[1] G.K. O'Neill, Phys. Rev. **102**, 1418 (1956).
[2] G.I. Budker, AIP Conf. Proc. **352**, 4 (1996).
[3] A.N. Skrinsky, AIP Conf. Proc. **352**, 6 (1996).
[4] D. Neuffer, Fermilab-FN-319 (1979).
[5] D. Neuffer, IEEE Trans. Nucl. Sci. **28**, 2034 (1981).
[6] A.N. Skrinskii and V.V. Parmhomchuk, Sov. J. Part. Nucl. **12**, 223 (1981).
[7] D. Neuffer, Part. Accel. **14**, 75 (1983).
[8] S. Chattopadhyay *et al.*, Nucl. Instrum. and Meth. A **350**, 53 (1994).
[9] D.V. Neuffer and R.B. Palmer, AIP Conf. Proc. **356**, 344 (1996).
[10] R. Palmer *et al.*, BNL-52503 (1996).
[11] C.M. Ankenbrandt *et al.*, Phys. Rev. ST Accel. Beams **2**, 081001 (2001).
[12] M. Alsharo'a *et al.*, Phys. Rev. ST Accel. Beams **6**, 081001 (2003).
[13] J.S. Berg *et al.*, Phys. Rev. ST Accel. Beams **9**, 011001 (2006).
[14] D. Cline and D. Neuffer, AIP Conf. Proc. **68**, 856 (1981).
[15] S. Geer, Phys. Rev. D **57**, 6989 (1998).
[16] N. Holtkamp *et al.*, Fermilab-Pub-00-108 (2000).
[17] S. Ozaki *et al.*, BNL-52623 (2001).
[18] C. Ankenbrandt *et al.*, Phys. Rev. ST Accel. Beams **12**, 070101 (2009).
[19] M. Apollonio *et al.*, J. Inst. **4**, 07001 (2009).
[20] R.J. Abrams *et al.*, IDS-NF Interim Design Report (2011).
[21] T. Sigurgeirsson, CERN/T/TS-2 (1952).
[22] E.D. Courant and H.S. Snyder, Ann. Phys. (N. Y.) **3**, 1 (1958).
[23] P.M. Lapostolle, IEEE Trans. Nucl. Sci. **18**, 1101 (1971).
[24] F.J. Sacherer, IEEE Trans. Nucl. Sci. **18**, 1105 (1971).
[25] J.D. Lawson, P.M. Lapostolle and R.L. Gluckstern, Part. Accel. **5**, 61 (1973).
[26] C. Lejune and J. Aubert, Adv. Elec. Elec. Phys. **S18**, 159 (1980).
[27] F. Neri and G. Rangarajan, Phys. Rev. Lett. **64**, 1073 (1990).
[28] R.C. Fernow, Muon Collider Note 280 (2003).
[29] M.J. Syphers, Fermilab-FN-0458 (1987).
[30] Lord Rayleigh, Phil. Mag. **3**, 338 (1902).
[31] H. Alfvén, Ark. Mat. Astro. Fys. **27A, no. 22** (1940).
[32] H. Alfvén, *Cosmical Electrodynamics* (Clarendon Press, 1950) Chap. 2.
[33] M.A. Green, AIP Conf. Proc. **372**, 100 (1996).
[34] N.V. Mokhov and A. Van Ginneken, AIP Conf. Proc. **441**, 320 (1998).
[35] C.T. Rogers *et al.*, Phys. Rev. ST Accel. Beams **16**, 040104 (2013).
[36] W.C. Turner, AIP Conf. Proc. **372**, 108 (1996).
[37] D. Neuffer and A. Van Ginneken, Proc. PAC01 , 2029.
[38] D. Neuffer, Fermilab pbar Note-104 (1980).
[39] E.D. Courant.
[40] K. Paul and C. Johnstone, AIP Conf. Proc. **721**, 329 (2004).
[41] X. Ding *et al.*, Phys. Rev. ST Accel. Beams **14**, 111002 (2011).
[42] O.M. Hansen and I. Efthymiopoulos, Proc. NuFACT12 , 60 (2012).
[43] R.J. Weggel *et al.*, Proc. IPAC11 , 1650 (2011).
[44] R.J. Weggel *et al.*, Proc. IPAC13 , 1514 (2013).
[45] D. Neuffer *et al.*, Proc. IPAC10 , 3500.
[46] N.V. Mokhov, Fermilab-FN-628 (2005).
[47] N.V. Mokhov and S.I. Striganov, AIP Conf. Proc. **896**, 50 (2007).
[48] R.C. Fernow, Proc. IPAC05 , 2651 (2005).
[49] R. Hagedorn, CERN-PS/RH9, secs. D-F (1955).
[50] A. Schoch, CERN-57-21, secs. 3-4 (1958).
[51] E.D. Courant, R.D. Ruth and W.T. Weng, AIP Conf. Proc. **127**, 294 (1985).
[52] G. Penn, Muon Collider Note 71 (2000).
[53] H.K. Sayed *et al.*, Proc. NAPAC13 , 547 (2013).
[54] J.C. Gallardo, Muon Collider Note 340 (2006).
[55] K.T. McDonald, *Analytic Forms for an Adiabatic Tapered Solenoid*, Tech. Rep. (Princeton U., 2010).